International Journal of Modern Physics A

Searches for new phenomena in final states with 3rd generation quarks using the ATLAS detector

Elham E Khoda,
on behalf of the ATLAS Collaboration *

Department of Physics and Astronomy, University of British Columbia,
2329 West Mall, Vancouver, BC V6T 1Z4, Canada
elham.e.khoda@cern.ch

Received 23 February 2021

Many theories beyond the Standard Model predict new phenomena, such as Z' and vector-like quarks, in final states containing bottom- or top-quarks. It is challenging to reconstruct and identify the decay products and model the major backgrounds. Nevertheless, such final states offer great potential to reduce the Standard Model backgrounds due to their characteristic decay signature. The latest search in the third-generation quark final states using the full Run-2 proton-proton collision data collected by the ATLAS experiment are presented. Particularly, the recent results of di-bjet and top-antitop resonance searches and dark matter produced in association with a top-quark are discussed in this proceedings. The associated improvements in b-quark and top-quark identification techniques are also highlighted.

Keywords: ATLAS; BSM; third-generation quarks, $t\bar{t}$ resonance; $b\bar{b}$ resonance; dark matter; b-tagging; top-tagging.

ATL-PHYS-PROC-2021-009
25 February 2021

1. Introduction

Despite its undisputed successes in describing the known elementary particles and their interactions, the standard model (SM) of particle physics is widely considered as an incomplete theory because it does not describe gravity and many experimental observations like dark matter, non-zero neutrino mass.[1,2] To address the shortcomings of the SM, several theories beyond the standard model (BSM) emerged in the last few decades. Many BSM theories such as quark composite models,[3,4] simplified dark matter (DM) models,[5,6] two-Higgs-doublet model (2HDM),[7] 2HDM with additional pseudoscalar,[8,9] models with extended gauge sector,[10–12] and Randall-Sundrum (RS) models[13,14] of warped extra dimensions predict new physics involving third-generation quarks. The third-generation quarks could shed some light on understanding the electroweak hierarchy problem and provide a window to new physics due to their large coupling with the Higgs sector. So the searches

for new physics in final states with third-generation quarks cover a large part of the Large Hadron Collider (LHC) physics program. These proceedings present the latest searches for the resonant production of bottom- and top-quarks and associated production of dark matter with a top-quark.[15–17] All these searches are performed with 139 fb^{-1} data collected by the ATLAS[18] detector from proton-proton collisions at the LHC between 2015 and 2018 at a centre-of-mass energy of $\sqrt{s} = 13$ TeV.

2. Searches for new resonances

Final states with two jets provide a simple system to search for new particles produced in the proton-proton collision and decay into quarks or gluons. One such new particle state is an excited quark, predicted by the composite models of quarks and leptons. The mass of excited quarks is expected to be at least a few hundred GeV or more. Such heavy states would instantaneously decay into an SM quark and a gluon producing a two jet resonance signature in the ATLAS detector. Some lepto-phobic models, such as the technicolor model,[19–21] predict new heavy particles with large coupling to the third-generation quarks. Such a heavy neutral particle will decay into the bottom- or top-quark pair. This section covers the final states with one or two b-quark(s), $t\bar{t}$. In addition to the complicated BSM models, a class of simplified dark matter model with a Z' mediator predicts enhanced production of $b\bar{b}$ and $t\bar{t}$. Final states with two jets could also be used to probe the RandallSundrum (RS) extra dimension model. The RS models include a Kaluza-Klein (KK) spin-2 graviton[22,23] that decays preferentially into quarks and gluons.

2.1. *Di-bjet resonance search*

Final states with one or two bottom-quarks are sensitive to the decay of a new heavy particle with stronger coupling to b-quarks or third-generation quarks in general. In addition to the aforementioned models, a simplified model with an additional $U(1)$ symmetry, known as the sequential standard model (SSM), also predicts Z' that decays into $b\bar{b}$. Two example Feynman diagrams of these benchmark signal processes are shown in Fig. 1.

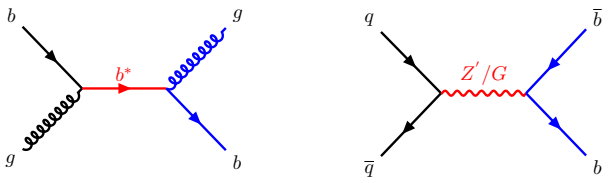

(a) Excited quark: b^* (b) Z' or Graviton (G)

Fig. 1. Example leading-order Feynman diagrams for production and decay of (a) excited b-quark (b^*) and (b) Z' or Graviton (G) into final states with at least one b-quark.

The ATLAS di-bjet search studies events with at least two jets out of which at least one is b-tagged.[15] In the analysis, events passing a single-jet trigger with a transverse momentum (p_{T}) threshold of 420 GeV are selected. In the selected events, jets are built by grouping the topological clusters using the anti-k$_t$ algorithm with a radius parameter of $R = 0.4$. Selected events are required to have at least two jets with p_{T} greater than 150 GeV in the central region within $|\eta| < 2.0$. In this case, the jets should be almost back-to-back in the transverse plane, so the azimuthal angle between the two leading jets is required to be greater than 1.0. Jets containing a b-hadron are identified using a deep-learning algorithm, DL1r. This algorithm is trained on the outputs of several low-level impact-parameter and secondary-vertex based algorithms. DL1r uses discriminating variables constructed by a recurrent neural network (RNNIP),[24] which exploits the spatial and kinematic correlations between tracks coming from a b-hadron. The di-bjet search is one of the first few analyses where this b-tagging algorithm[25] is used. DL1r performs much better on the high p_{T} jet compared to the previously used algorithm. To suppress the QCD multijet background, half of the absolute rapidity difference between the two leading jets, $|y^*| = |y_1 - y_2|/2$, is required to be less than 0.8.

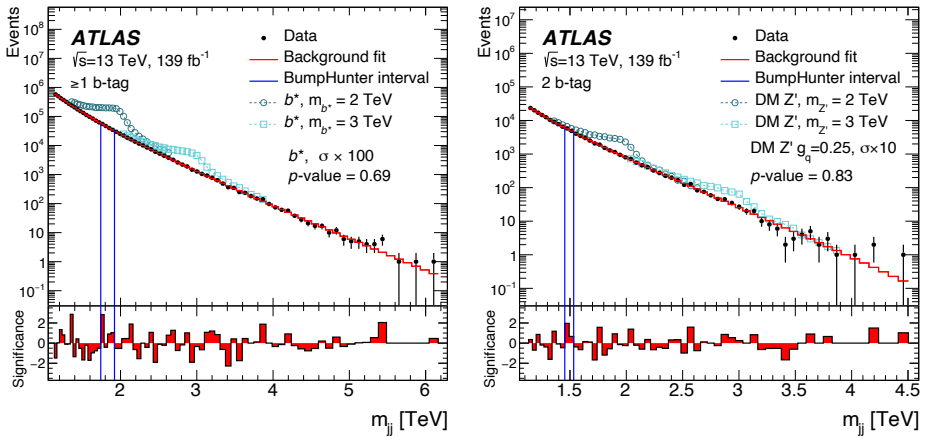

(a) ≥ 1 b-tag (b) 2 b-tag

Fig. 2. Dijet invariant mass distributions in the signal regions with (a) at least one b-tagged jet and (b) two b-tagged jets. The vertical lines indicate the most discrepant interval identified by the BumpHunter test, and the corresponding p-values are shown on the plots. The BumpHunter local significances are shown in the lower panel. Some representative signal models are also overlaid on the dijet distributions.[15]

The invariant mass of the two leading jets (m_{jj}) is used as the main discriminant in this search. The dominant SM background contribution comes from the QCD multijet processes. The m_{jj} distribution in the simulated multijet processes describes the shape in data well, but the normalization does not match. So, the simulated

events are not used to estimate the SM background. It is observed that the shape of the SM m_{jj} spectrum is smoothly falling and can be described by analytic functions. So, the background m_{jj} distribution is modelled by fitting the data with the following polynomial function

$$f(x) = p_0(1-x)^{p_1} x^{p_2+p_3 \log(x)} \ , \tag{1}$$

where $x = m_{jj}/\sqrt{s}$, and p_i are the fit parameters. It is found that the function cannot describe the full mass distribution. The background is therefore estimated by fitting the m_{jj} spectrum in small windows at a time. The size of the window is the maximum interval with global BumpHunter p-value[26] greater than 0.01. The BumpHunter p-value is computed to estimate the statistical significance of any localized excess in the m_{jj} distributions in data relative to the fitted background. The large p-value indicates the fit is describing data well. Fig. 2 shows the m_{jj} distributions in the two signal regions along with the BumpHunter local significances. The most discrepant intervals are indicated by the vertical blue lines. The global p-values of 0.69 and 0.83 indicates good agreement between data and background.

Since no significant deviation from the expected background is observed, upper limits on signal cross-section times branching ratio is set at 95% confidence level (CL) using a Frequentist framework. While calculating the limits, systematic uncertainties are taken into account. The statistical uncertainty of the fit coming from the limited size of the data sample and the uncertainty due to the choice of fit function are considered as background uncertainties. On the other hand, in the simulated signal samples, the main contributions come from the modelling of the jet energy scale, jet energy resolution, and b-tagging efficiency. For signals, the effects coming from the choice of the parton distribution function (PDF) and PDF scale are considered. As shown in Fig. 3, b^* and Z' with masses below 3.2 TeV and 2.7 TeV, respectively, are excluded at 95% CL.

2.2. *Top-antitop resonance search in boosted all-hadronic final state*

Top-quark, the heaviest elementary particle of the SM with a mass close to the electroweak symmetry breaking, could provide a window to the new physics through its large coupling to the Higgs sector. Nonetheless, many BSM models predict new heavy particles with large coupling to the top-quarks. The topcolor-assisted-technicolor (TC2) is one such top-philic model with a heavy Z'_{TC2} particle preferentially couple with top-quarks. Also, a large class of simplified dark matter models, mentioned in the previous section, predict heavy mediator particles (Z') that couple with both dark matter particles and the SM particles. As a result, these mediators could decay into a top-quark pair.

In this analysis,[16] the $t\bar{t}$ all-hadronic final state where both the W bosons, coming from top-quarks, decay hadronically. The all-hadronic final state benefits

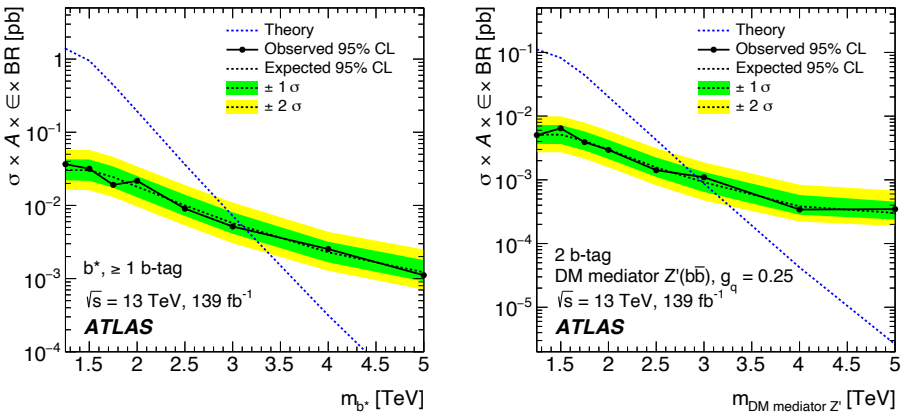

(a) b^* (b) DM $Z'(b\bar{b})$

(c) SSM $Z'(b\bar{b})$ (d) $G(b\bar{b})$

Fig. 3. 95% CL upper limit on the signal cross-section time branching ratio as a function of mass of (a) b^*, (b) Z' of the dark-matter mediator model, (c) Z' of the SSM, and (d) Graviton.[15]

from the largest top-quark decay branching ratio. But the reconstruction of the $t\bar{t}$ system and identification of a new physics signal are challenging due to the large SM multijet background. However, if the momentum of a top-quark is sufficiently high, its decay products come close enough to be reconstructed as a single large-radius (large-R) jet. Therefore this analysis focuses only on the high momentum (boosted) top-quarks and studies events with $m_{t\bar{t}}^{\mathrm{reco}}$ above 1.3 TeV. The analysis uses events selected by the large-R jet triggers requiring at least one large-R jet with $p_{\mathrm{T}} >$ 360-460 GeV, depending on the data-taking period. The large-R jets are built by grouping the topological clusters using the anti-k$_t$ algorithm with a radius parameter $R = 1.0$. Events with at least two large-R jets are selected if the leading

two jets have $p_{\mathrm{T}} > 500$ GeVand $p_{\mathrm{T}} > 350$ GeV, respectively. Events containing an isolated lepton are removed to be orthogonal to the searches using the other top-decay channels. Since the top-quarks coming from a heavy particle decay are expected to be back-to-back in the transverse plane, the difference in their azimuthal angle is required to be greater than 1.6. In addition, to reduce t-channel multijet production a rapidity distance cut of $|\Delta y_{jj}| < 1.8$ is applied. The two leading large-R jets in the selected events are required to be identified as top-quarks. Large-R jets originated from the top-quark decay are identified with a DNN-based classifier,[27] which uses jet-level discriminants like N-subjettiness,[28,29] splitting scale,[30] energy correlation function,[31,32] jet mass, p_{T}, and many more as inputs. In this analysis, the DNN top-tagger with 80% signal efficiency is used. The selected events are further categorized into two signal regions (SR) depending on the number of b-tagged jets associated with the top-tagged large-R jets. b-tagging is performed on the track jets using a similar DNN-based algorithm (DL1) described in the previous section. If only one of the two top-tagged jets has at least one b-tagged track jet within $\Delta R < 1.0$, then the event belongs to the 1 b-tagged SR (SR1b). Events, where both top-jets are associated with b-jets, are categorized into the 2 b-tagged SR (SR2b). A background control region without any b-tagging requirement is also defined to study the SM multijet background (without top-quarks).

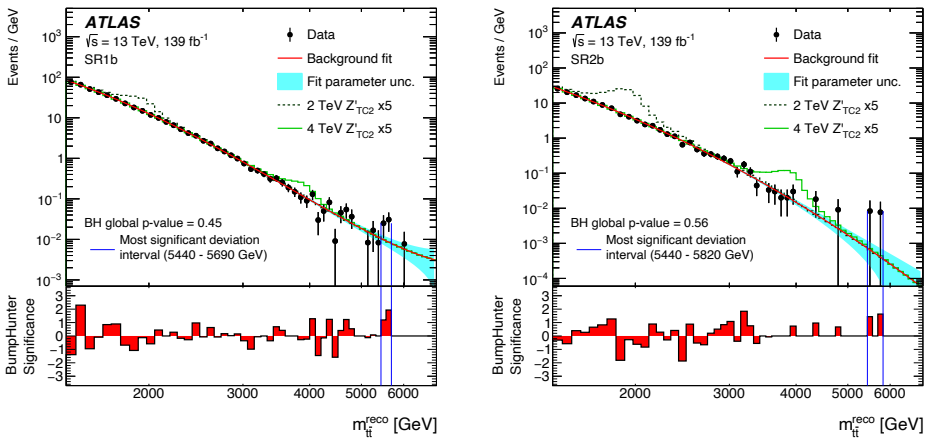

(a) ≥ 1 b-tag (b) 2 b-tag

Fig. 4. Observed $m_{t\bar{t}}^{\mathrm{reco}}$ distributions in (a) SR1b and (b) SR2b shown together with the fitted backgrounds. The shaded band around the fit shows the fit parameter uncertainty. The predicted Z'_{TC2} signal distributions with masses of 2 and 4 TeV are superimposed on the background after multiplying by a factor of 5. The lower panel shows the BumpHunter local significances. The two vertical lines indicate the most significant interval.[16]

The main backgrounds come from the SM $t\bar{t}$ pair production and other QCD multijet process. Although the simulated $t\bar{t}$ process describes the data well, simulations of other QCD multijet processes are not accurate. So, a data-driven method

is used to estimate the background. The main discriminant is the invariant mass of the $t\bar{t}$ system ($m_{t\bar{t}}^{\text{reco}}$). It is observed that the shape of the $m_{t\bar{t}}^{\text{reco}}$ distribution, coming from all the SM processes, can be described by an analytic function. So the background contribution is estimated by fitting the $m_{t\bar{t}}^{\text{reco}}$ spectrum using the four-parameter polynomial function described in Eq. 1. Unlike the dijet resonance search, the background is estimated by fitting the full range of the distribution at once. The background is estimated separately in the two signal regions. Fig. 4 shows the observed $m_{t\bar{t}}^{\text{reco}}$ distribution in the two SRs with the fits. The cyan bands around the fits represent the fit parameter uncertainty. The fake signal extracted by the fit method in the absence of any real signal is called the spurious signal. The spurious signal is estimated carefully in this analysis and used as a background uncertainty as a function of $m_{t\bar{t}}^{\text{reco}}$. The BumpHunter local significances shown in Fig. 4 are almost always less than 2σ and the global p-values are around 0.5, indicating no hint of new physics.

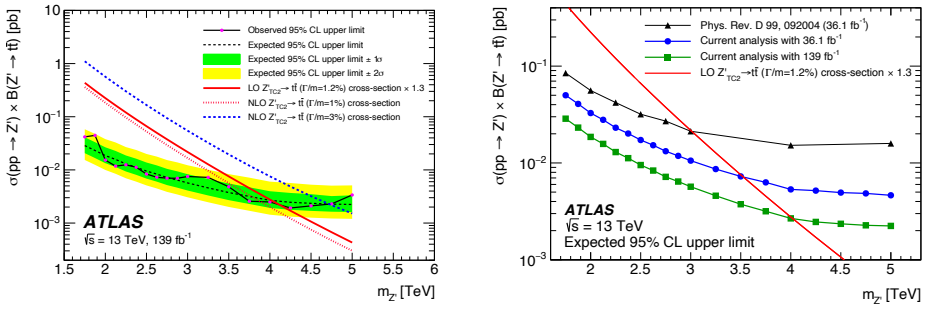

(a) (b)

Fig. 5. (a) 95% CL upper limits on the cross-section times branching ratio of the $Z'_{TC2} \to t\bar{t}$ as a function of Z'_{TC2} mass. NLO theory cross-sections for the Z'_{TC2} with 1%, 1.2%, and 3% width are shown in the red dotted, red solid, and blue dashed lines, respectively. (b) Comparison of the expected upper limits on signal as a function of Z'_{TC2} mass. The triangle markers show the expected limits from the previous analysis using 36.1 fb^{-1} of the 2015-2016 data. The circle markers show the expected limits obtained by applying the current analysis to 36.1 fb^{-1} of the 2015-2016 data. The square markers show the current expected limits obtained using 139 fb^{-1} of the full Run-2 data.[16]

In the absence of any new physics, limits are set on the signal cross-section times branching ratio ($\sigma \times B$) at 95% CL. A simultaneous binned maximum-likelihood fit is performed in the two signal regions. The final hypothesis test is done using a Frequentist approach. The Z'_{TC2} model with different width, $\Gamma/m = 1\%, 1.2\%$ and 3% are used to interpret the limits. The expected and observed upper limits on the $\sigma \times B$ of $Z'_{TC2} \to t\bar{t}$ are presented in Fig. 5a. Z'_{TC2} particles with 1.2% relative width and masses below 4 TeV are excluded at 95% CL. The expected sensitivity of this search was limited by the large spurious signal uncertainty above 4.5 TeV. Fig. 5b shows the analysis improvements compared to the previous analysis. The

cross-section limits improved by a factor of two due to new background estimation strategy and usage of efficient b-tagging and top-tagging methods, it further improved by another factor of two after using four times more data.

2.3. *Dark matter interpretation*

The results from the dijet and $t\bar{t}$ resonance search are also interpreted[33] with the simplified dark matter model with axial-vector (Z'_A) and vector (Z'_V) mediator, proposed by the LHC dark matter working group.[9] These mediators couple the dark sector to the SM sector. So any enhanced production of $b\bar{b}$ and $t\bar{t}$ could come from the decay of these Z' meditors. Fig. 6 shows the 95% CL upper limits on the quark coupling is shown as a function of axial-vector mediator mass $m_{Z'_A}$. Dijet and $t\bar{t}$ resonance search contours are shown in light blue and purple lines. Similar two dimensional limit contours are made for dark matter mass (m_χ) as a function of the mediator mass ($m_{Z'_A}$ or $m_{Z'_V}$) and can be found in Ref. 33. The dijet resonance search sets the best limit on both Z'_A and Z'_V mass, which is around 3.6 TeV.

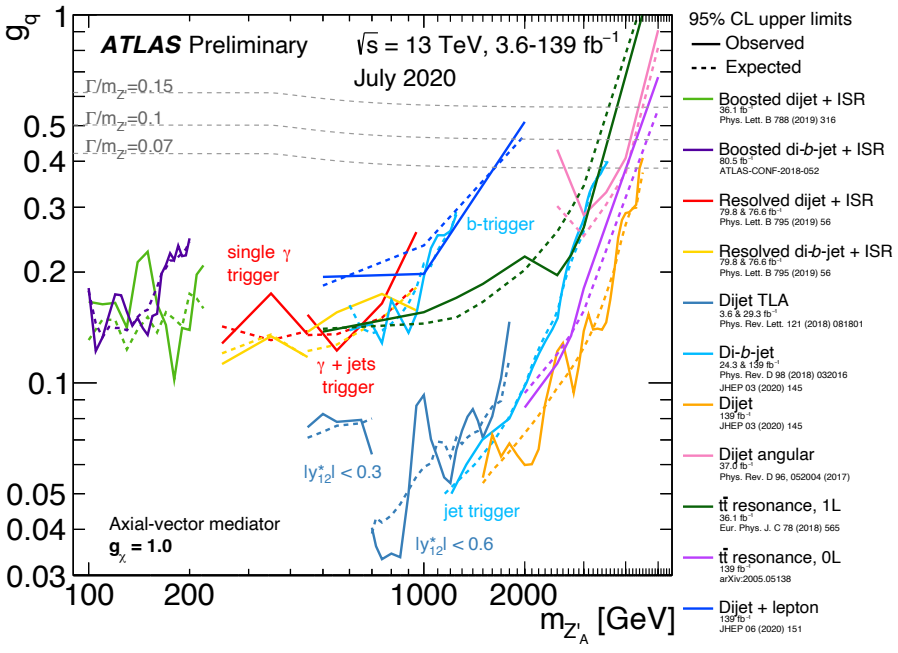

Fig. 6. Hadronic resonance search contours for 95% CL upper limits on the quark coupling, g_q as a function of the mediator mass, $m_{Z'_A}$.[33]

3. Search for dark matter produced in association with a single top quark

The nature and properties of dark matter (DM) are still unknown. One of the widely used hypothesis is that dark matters are weakly interacting massive particles (WIMP). Collider experiments like ATLAS are not designed to detect such WIMP-like DM particles directly. So different complementary approaches are used to search for DM produced in association with the visible particles. The experimental signature for a DM candidate is missing transverse energy (MET). A simplified DM model involving an extended 2 Higgs Doublet Model (2HDM) with an additional pseudoscalar mediator (a) is considered in this search. This model predicts two scalar Higgs boson h and H, two pseudoscalars A and a, and charged scalars $H^{\pm}$. The pseudoscalar a is a mediator between the DM particles, χ, and the SM sector. This analysis explores the processes, where the pseudoscalar mediator is produced in association with a single top-quark for the first time at the LHC. Fig. 7 shows different signal processes where a decays into two DM particles considered in this analysis.

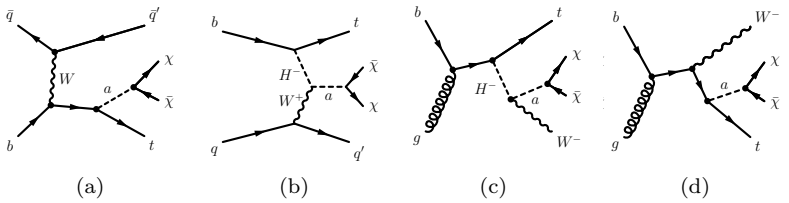

Fig. 7. Example LO Feynman diagram of pair production of DM particle based on 2HDM+a model consider in this analysis.

The presence of a top quark and W bosons leads to final states with various combinations of leptons, jets, and b-jets. So to maximize sensitivity, the search is performed in three independent analysis channels. The tW_{1L} channel targets tW+DM events, where one of the W bosons decays leptonically. Whereas, in the tW_{2L} channel both W bosons decay leptonically. The third channel tj_{1L} is designed to target the t-channel production of DM in association with a leptonically decaying top-quark and addition jets.

3.1. *Single-lepton tj_{1L} channel*

The final states containing a top-quark with jets use a combination of single-lepton and MET (E_T^{miss}) triggers. Events with exactly one lepton (electron or muon) are selected first for this region if they also contain 1-4 jets and 1-2 b-jets. To further improve sensitivity a boosted decision tree (BDT) is trained to distinguish signals from the background. Different signal models are combined to train the BDT to ensure it learns a wide range of signal parameter space. The BDT takes nine input

variables related to the leading jet, leading lepton and b-jet system, and transverse masses. Events with a BDT score above 0.6 are selected. Two CRs are designed to estimate the dominant backgrounds coming from the $t\bar{t}$ and W+jets events. Finally, a binned distribution of the BDT score with four bins is used in the statistical analysis. The BDT score distribution is shown in Fig. 8.

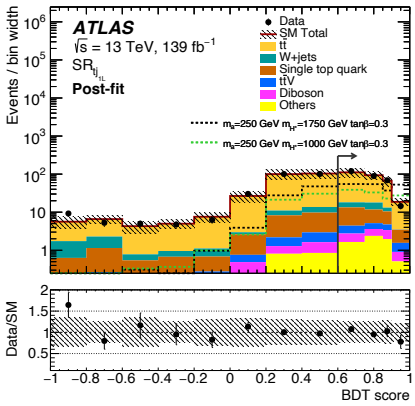

Fig. 8. BDT score distribution in the tj_{1L} region where observed data are compared to the post-fit SM predictions. The four bins of this distribution above score of 0.6 are used in the statistical analysis.[17]

3.2. *Single-lepton tW_{1L} channel*

Events are required to pass the MET trigger which is fully efficient for reconstructed $E_T^{\text{miss}} > 250$ GeV. Only events with a lepton and at least three jets, one of which is a b-jet are selected. High E_T^{miss} and transverse mass values are required to separate signals from backgrounds. Further improvements in the sensitivity come from variables like stransverse mass and asymmetric stransverse mass,[17] which relates the transverse mass of DM particles to the transverse mass of the particle it decayed from. All the SM background processes are estimated using simulation. Furthermore, dedicated control regions (CR) are designed to estimate the normalization of the $t\bar{t}$ and W+jets backgrounds. Finally, a binned E_T^{miss} distribution with five bins, shown in Fig. 9, is used for the statistical analysis.

3.3. *Dilepton tW_{2L} channel*

A combination of dilepton triggers is used to select events in this channel. Events are required to have exactly two opposite signed leptons with at least one signal jet, at least one of which must be b-tagged. To further reduce the background, transverse mass, angular separations, and different combinations of b-jet and lepton masses are

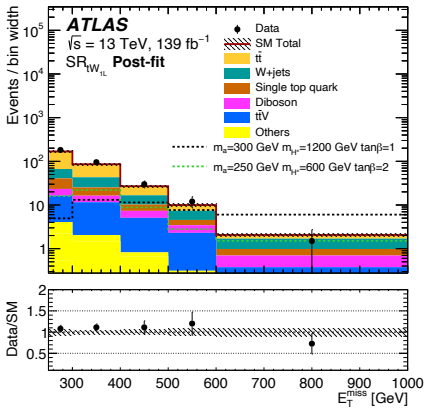

Fig. 9. E_T^{miss} distribution in the tW_{1L} channel, where observed data are compared to the post-fit SM predictions. These 5 bins of MET distribution is used for statistical analysis.[17]

used. All the SM backgrounds are estimated using simulation, and their CRs are defined for the $t\bar{t}$, $t\bar{t}V$ (with $V = W$ or Z boson), and diboson backgrounds. This channel is included as a single bin signal region in the statistical fit.

3.4. *Results*

The analysis considers several sources of systematic and theoretical uncertainties for signal and background processes. The impact of these uncertainties is reduced through the normalization of the dominant backgrounds in the CRs. Dominant detector-related systematic uncertainties arise from the jet energy scale and resolution, and the b-tagging efficiency. Modelling uncertainties are also included while performing the statistical analysis. The event yields and the significances in different SRs of the three analysis channels are presented in Fig. 10. No significant deviations compared to expected yields are observed in the data.

In the absence of new physics exclusion limits are set on the signal parameters m_a, $m_{H^\pm}$ and the ratio of the vacuum expectation values of the Higgs boson doublets tan β of the 2HDM+a models. To reduce the parameter space the masses of the additional Higgs bosons (H, $H^\pm$, A) are set to be equal. The quartic couplings between the scalar doublets and the a boson are also set to be equal. To maximize sensitivity a statistical combination of the tW_{1L} and tW_{2L} channels are done. Two sets of samples are considered varying either the (m_a, $m_{H^\pm}$) and setting $\tan\beta = 1$, or varying the ($m_{H^\pm}$, $\tan\beta$) and setting $m_a = 250$ GeV. Fig. 11a and 11b show the observed and expected exclusion contours as a function of (m_a, $m_{H^\pm}$) and ($m_{H^\pm}$, $\tan\beta$), respectively, for the tW_{1L} and tW_{2L} channels and their combination. Assuming the DM mass (m_χ) of 10 GeV and coupling (g_χ) of 1, masses of a below 160 GeV are excluded for $m_{H^\pm} \in$ [400-1400] GeV at 95% CL, and up to 3.2 TeV for $m_{H^\pm}$ around 800 GeV. In the other case, where $m_a = 250$ GeV, all values of

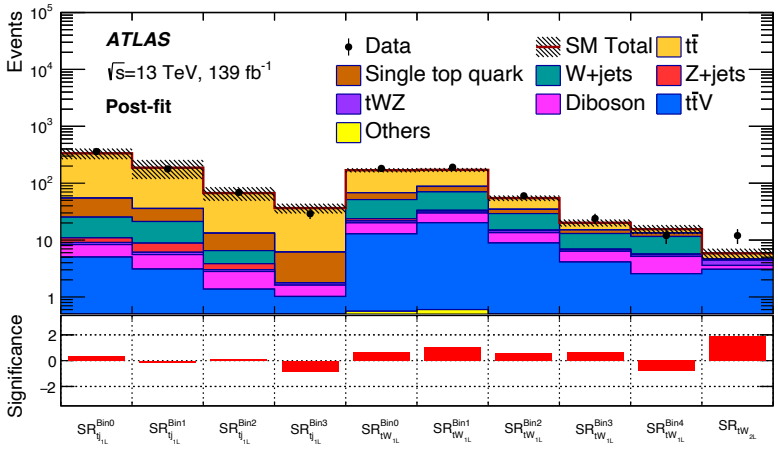

Fig. 10. Results of background-only fit extrapolated to all the SRs, where the normalizations of the backgrounds are obtained from the CRs. Observed number of events and the predicted background are shown in the uppper panel, and the lower panel shows the significance in each SRs.[17]

$m_{H^\pm}$ between 550 GeVand 1150 GeVare excluded for $\tan\beta$ around and below unity.

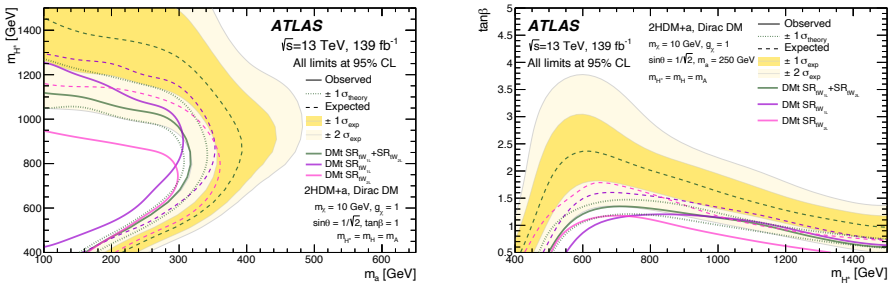

(a) (b)

Fig. 11. 95% CL exclusion contours for (a) the charged Higgs mass ($m_{H^\pm}$) as a function of the pseudoscalar mass (m_a) for an assumed DM mass (m_χ) of 10 GeV, DM coupling (g_χ) of 1, and $\tan\beta = 1$ (b) $\tan\beta$ as a function of $m_{H^\pm}$ where m_a is assumed to be 250 GeV.[17]

The $tj1L$ channel has smaller sensitivity compared to the other two channels due to smaller t-channel production cross-section. Fig. 12 shows the observed and expected limits on t-channel DM production cross-section at 95% CL as a function of $m_{H^\pm}$ for two representative values of $\tan\beta$ for $m_a = 250$ GeV. For $\tan\beta = 0.3$, $m_{H^\pm}$ values are excluded above 900 GeV.

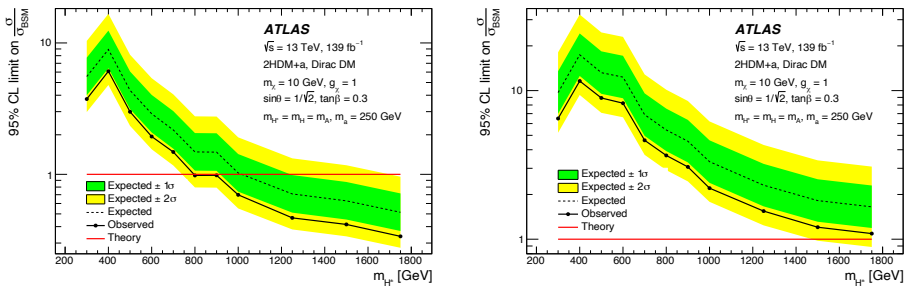

(a) (b)

Fig. 12. 95% CL upper limits on signal cross-section as a function of charged Higgs mass ($m_{H^\pm}$) in the tj_{1L} channel for signal model with pseudoscalar mass (m_a) of 250 GeVand $\tan\beta$ = (a) 0.3 and (b) 0.5.[17]

4. Conclusions

The third-generation quarks show several distinct properties like their higher masses and couplings to the SM Higgs sector. The reasons behind these observations are still not fully understood. So careful studies of the final states with third-generation quarks could give us hints for new physics. The proceedings present only three out of many such exciting searches in ATLAS. The b-quarks and the top-quarks develop characteristic signatures in the detector that are highly discriminating and are used to identify them in the first place. Machine learning (ML) methods exploit these features more effectively and identify the b-and the top-quarks more efficiently. Search results in the dijet and $t\bar{t}$ final states improved significantly after using DNN-based b- and top-tagging methods. Several other advanced analysis and background estimation techniques, discussed here, also helped to improve the sensitivity. With the rapid integration of different advanced ML techniques to high-energy physics research, these analyses are expected to use many more novel techniques in the future. Although no hint of new physics is observed, more stringent limits are placed on the signal cross-sections predicted by the BSM models.

References

1. D. E. Morrissey, T. Plehn, and T. M. Tait, Physics searches at the LHC, *Phys. Rept* **512**, 1 (2012).
2. Y. Gershtein et al. Working Group Report: New Particles, Forces, and Dimensions, *Community Summer Study 2013: Snowmass on the Mississippi.* (2013)
3. U. Baur, I. Hinchliffe, and D. Zeppenfeld, Excited Quark Production at Hadron Colliders, *Int. J. Mod Phys. A* **02** 1285 (1987).
4. Excited-quark and -lepton production at hadron colliders, *Phys. Rev. D* **42** 815 (1990).
5. A. Boveia et al., Recommendations on presenting LHC searches for missing transverse energy signals using simplified s-channel models of dark matter, *Phys. Dark Univ.* **27** 100365 (2020).
6. D. Abercrombie et al., Dark Matter Benchmark Models for Early LHC Run-2 Searches:

Report of the ATLAS/CMS Dark Matter Forum, *Phys. Dark Univ.* **27** 100371 (2020).
7. G. C. Branco et al., Theory and phenomenology of two-Higgs-doublet models, *Phys. Rept.* **516** 1 (2012).
8. M. Bauer, U. Haisch and F. Kahlhoefer, Simplified dark matter models with two Higgs doublets: I. Pseudoscalar mediators, *JHEP* **2017** 138 (2017).
9. T. Abe et al., LHC Dark Matter Working Group: Next-generation spin-0 dark matter models, *Phys. Dark Univ.* **27** 100351 (2020).
10. P. Langacker, The Physics of Heavy Z' Gauge Bosons, *Rev. Mod. Phys.* **81** 1199 (2009).
11. C.-W. Chiang, T. Nomura, and K. Yagyu, Phenomenology of E_6-inspired leptophobic Z' boson at the LHC, *JHEP* **05** 106 (2014).
12. E. Eichten, I. Hinchliffe, K. Lane, and C. Quigg, Supercollider physics, *Rev. Mod. Phys.* **56** 579 (1984).
13. L. Randall and R. Sundrum Large Mass Hierarchy from a Small Extra Dimension, *Phys. Rev. Lett.* **83** 3370 (1999).
14. B. Lillie, L. Randall and L.-T. Wang, The Bulk RS KK-gluon at the LHC, *JHEP* **09** 074 (2007).
15. ATLAS Collaboration, Search for new resonances in mass distributions of jet pairs using 139 fb^1 of pp collisions at $\sqrt{s} = 13$ TeV with the ATLAS detector, *JHEP* **2020**, 145 (2020).
16. ATLAS Collaboration, Search for $t\bar{t}$ resonances in fully hadronic final states in pp collisions at $\sqrt{s} = 13$ TeV with the ATLAS detector, *JHEP* **2020**, 61 (2020).
17. ATLAS Collaboration, Search for dark matter produced in association with a single top quark in $\sqrt{s} = 13$ TeV pp collisions with the ATLAS detector, arXiv:2011.09308 [hep-ex] (2020).
18. ATLAS Collaboration, The ATLAS experiment at the CERN large hadron collider, *JINST* **3**, S08003 (2008).
19. C. T. Hill and S. J. Parke, Top quark production: Sensitivity to new physics, *Phys. Rev. D* **49** 4454 (1994).
20. C. T. Hill, Topcolor assisted technicolor, *Phys. Lett. B* **345** 483 (1995).
21. R. M. Harris and S. Jain, Cross sections for leptophobic topcolor Z' decaying to top-antitop, *EPJC* **72** 2072 (2012).
22. K. Agashe, H. Davoudiasl, G. Perez and A. Soni, Warped Gravitons at the LHC and Beyond, *Phys. Rev. D* **76** 036006 (2007).
23. A. L. Fitzpatrick, J. Kaplan, L. Randall and L.-T. Wang, Searching for the KaluzaKlein Graviton in Bulk RS Models, *JHEP* **09** 013 (2007).
24. ATLAS Collaboration, Optimisation and performance studies of the ATLAS b-tagging algorithms for the 2017-18 LHC run, ATL-PHYS-PUB-2017-013 (2017)
25. ATLAS Collaboration, ATLAS b-jet identification performance and efficiency measurement with $t\bar{t}$ events in pp collisions at $\sqrt{s} = 13$ TeV, *EPJC* **79** 11 (2019)
26. G. Choudalakis, On hypothesis testing, trials factor, hypertests and the BumpHunter, arXiv: 1101.0390 [physics.data-an] (2011).
27. ATLAS Collaboration, Performance of top-quark and -boson tagging with ATLAS in Run 2 of the LHC, *EPJC* **79** 375 (2019)
28. J. Thaler and K. Van Tilburg, Identifying boosted objects with N-subjettiness, *JHEP* **2011**, 15 (2011).
29. J. Thaler and K. Van Tilburg, Maximizing boosted top identification by minimizing N-subjettiness, *JHEP* **2012**, 93 (2012).
30. J. Thaler and L.-T. Wang, Strategies to Identify Boosted Tops, *JHEP* **2008** 92 (2008).
31. A. J. Larkoski, G. P. Salam and J. Thaler, Energy correlation functions for jet sub-

structure, *JHEP* **2013** 108 (2013).
32. A. J. Larkoski, I. Moult and D. Neill, Power counting to better jet observables, *JHEP* **2014** 09 (2014).
33. ATLAS Collaboration, Dark matter summary plots for s-channel mediators, ATL-PHYS-PUB-2020-021 (2020).